THE
PHYSICAL REVIEW

A journal of experimental and theoretical physics established by E. L. Nichols in 1893

SECOND SERIES, VOL. 166, NO. 2 10 FEBRUARY 1968

Properties of Rubidium Atoms Trapped in a Solid Argon Matrix*

STUART L. KUPFERMAN† AND F. M. PIPKIN
Lyman Laboratory of Physics, Harvard University, Cambridge, Massachusetts

(Received 7 August 1967)

This paper reports studies of the optical absorption spectrum and the X-band electron spin resonance spectrum of rubidium atoms trapped in an argon matrix. The samples were formed by deposition from a mixed beam of the two constituents onto a cold plate. The optical absorption measurements showed two groups of lines. The red group, whose absorption lines are near those of the free atom, has a triplet structure; the blue group, whose absorption lines are shifted roughly 1650 cm^{-1} to the blue, has four lines. The ESR measurements showed three major trapping sites. A motorized circular polarizer was used to measure the differential absorption of right and left circularly polarized light. By monitoring the differential absorption of right and left circularly polarized light in the presence of a microwave field, a correlation was found between the optical absorption sites and the microwave absorption sites. A crystal-field model is employed in an attempt to fit the data and to understand the nature of the sites.

INTRODUCTION

WORK at this laboratory with alkali-metal atoms trapped in rare-gas matrices was started several years ago in an effort to produce nuclear orientation through optical pumping in solids.[1,2] *A priori* such a line of investigation is promising since the rare gases form weakly bound molecular crystals. Thus one has the hope of retaining the high optical absorption of the alkali atoms without the quenching of the orbital angular momentum such as occurs in the alkali-halide F centers and which makes them unsuitable for optical pumping. The first attempts at optical pumping were unsuccessful; as a result a further study was undertaken to understand the environment of an alkali atom in an inert-gas matrix. Work on this problem in this and other laboratories has consisted primarily of studies of the electron spin and optical absorption spectra of different alkali-metal–rare-gas combinations under various conditions of growth and preservation.[2–8]

Optical absorption studies have indicated the existence of two triplet absorption lines in the vicinity of the free alkali atom first principal series doublet. One triplet is close to the doublet position and the other is shifted several hundred angstroms to the blue. These results have been interpreted to mean that there are two types of trapping sites in the rare-gas matrix and that the field at each of these sites is of sufficiently low symmetry to remove the threefold orbital degeneracy of the p configuration. Electron spin resonance (ESR) studies have shown several lines in the vicinity of the free-atom ESR lines. The number of lines seen has been observed to vary with the alkali-metal–rare-gas matrix combination and with the growth conditions of the sample. No simple explanation for the multiplicity of trapping sites has been proposed.

In the previous work carried out in this laboratory, it was concluded that the rubidium atoms were not trapped in substitutional sites and a crystal-field model was used in an attempt to understand the nature of the sites. Since the general crystal-field expression involves three independent parameters and the data only gave two independent splittings, it was necessary to assume that one of the terms of the field was zero. In order to simplify the problem it was assumed that

* Research supported in part by a grant from the National Science Foundation.

† Present address: Manned Spacecraft Center, Houston, Tex.

[1] W. Weyhmann and F. M. Pipkin, Phys. Rev. **137**, A490 (1965).

[2] W. Weyhmann, thesis, Harvard University, 1963 (unpublished).

[3] E. L. Cochran, V. A. Bowers, S. N. Foner, and C. K. Jen, Phys. Rev. Letters **2**, 43 (1959).

[4] M. McCarty, Jr., and G. W. Robinson, Mol. Phys. **2**, 415 (1959).

[5] S. N. Foner, E. L. Cochran, V. A. Bowers, and C. K. Jen, J. Chem. Phys. **32**, 963 (1960).

[6] C. K. Jen, V. A. Bowers, E. L. Cochran, and S. N. Foner, Phys. Rev. **126**, 1749 (1962).

[7] J. P. Goldsborough and T. R. Koehler, Phys. Rev. **133**, A135 (1964).

[8] B. Meyers, J. Chem. Phys. **43**, 2986 (1965).

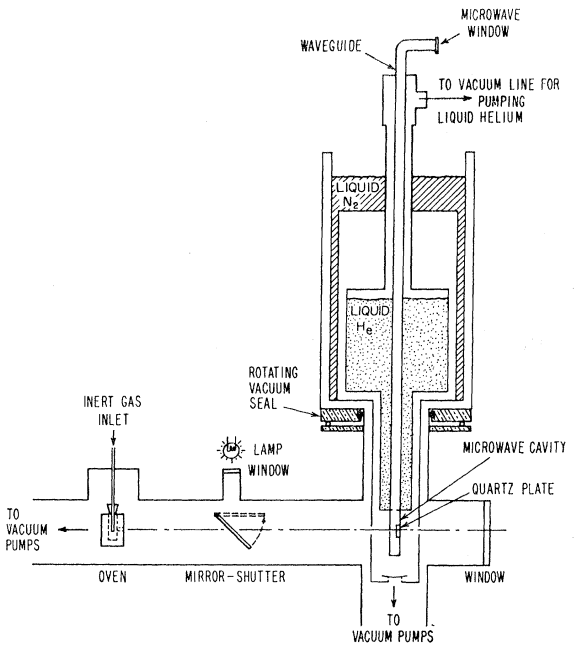

FIG. 1. Diagram showing the vacuum system, the rubidium-argon oven source, and the helium Dewar

the crystal-field potential possessed a twofold axis of symmetry and could be decomposed into terms of cubic and rhombic symmetry. Even with this simplification it was possible to find three forms of solution which would fit all of the data for eight combinations of Na, K, Rb, and Cs in Ar, Kr, and Xe. In order to learn more about the nature of the sites it is necessary to have more detailed information. One useful probe is the differential absorption of right and left circularly polarized light when the atoms are at helium temperatures. Under these conditions the ground state of the atom is polarized and the differential absorption of right and left circularly polarized light depends upon the quenching of the angular momentum of the excited p state. Thus the differential absorption of circularly polarized light gives a measure of how the excited-state wave functions of the trapped atom are to be constructed out of the free-atom wave functions. Using this information it is possible to determine more completely the crystal-field parameters and the nature of the sites.

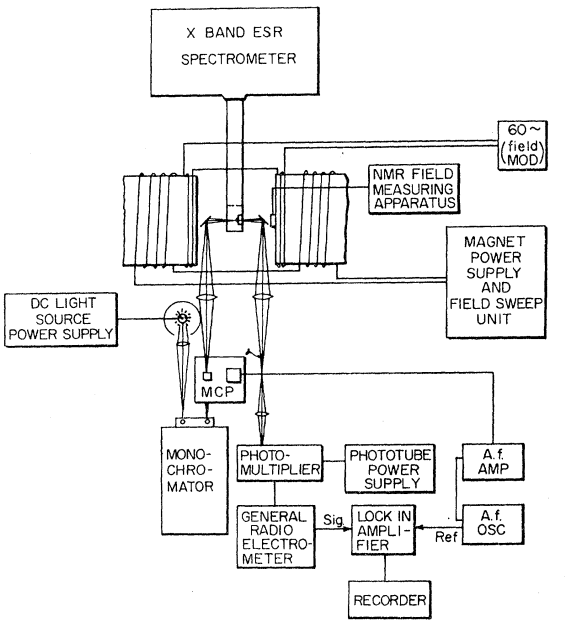

FIG. 2. Block diagram showing the various components of the apparatus.

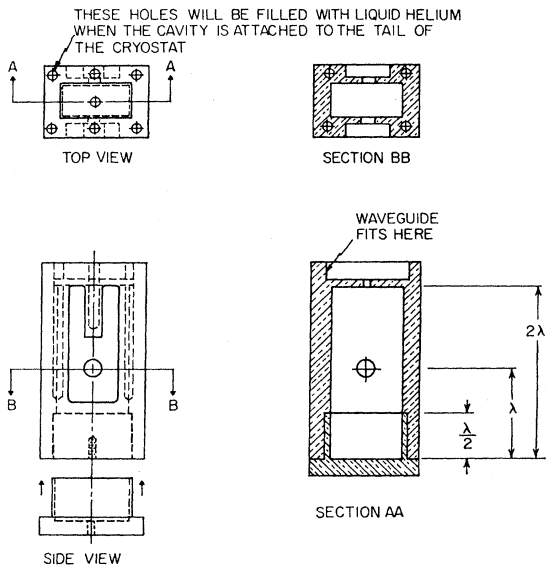

FIG. 3. Diagram showing the construction of the X-band cavity. The cavity was made by electroforming copper on an aluminum mandrel.

This paper reports work carried out to investigate the nature of the trapping sites through observations of the way in which rubidium atoms in an argon matrix absorb circularly polarized light and through observations of the interaction between the sites observed in ESR studies and those observed optically through simultaneous observations of both types of spectra. This paper describes in turn the equipment used to grow and study the trapped atoms, the theory of light absorption by trapped atoms, the procedures used for collecting and reducing the data, and the results of the measurements.

APPARATUS

The apparatus was designed so that one could grow and preserve samples consisting of rubidium atoms trapped in argon matrices and then make on these samples simultaneous observations of the optical and

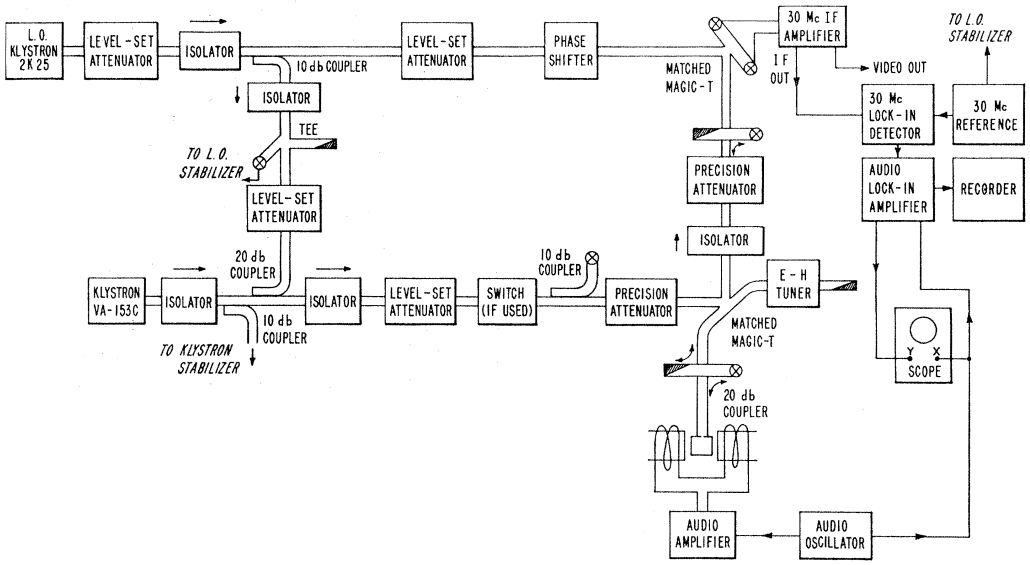

FIG. 4. A block diagram of the electron paramagnetic resonance spectrometer.

electron spin resonance (ESR) spectra. The basic components were a vacuum and Dewar system, an electromagnet and magnet power supply, field-measuring equipment, an ESR spectrometer, and an optical spectrometer. Figure 1 shows the helium Dewar and sample-growing apparatus; Fig. 2 shows the block diagram of the apparatus used for studying the samples.

The samples were grown by directing a single-beam mixture of argon and rubidium vapor against a 2-mm-thick, single-crystal quartz plate which was cooled to liquid-helium temperature and surrounded by walls which were cooled to liquid-helium temperature. The gas-metal mixture was obtained by passing the argon through a molecular-beam type oven which was filled with rubidium vapor (see Fig. 1). The rubidium concentration in the beam was controlled by adjusting the oven temperature.

The quartz plate was fastened with silicon vacuum grease against the center of the broad face of a TE_{012} X-band microwave cavity. A quartz single-crystal plate was used because of its high thermal conductivity at liquid-helium temperature. Holes $\frac{3}{16}$ in. in diam were drilled in the cavity faces opposite to and behind the plate to admit the plating mixture and to allow a clear optical path through the sample. The microwave cavity was soft-soldered to the tail of the inner pot of a liquid-helium cryostat with the waveguide running down through the liquid helium as shown in the Fig. 1. The waveguide was evacuated through the cavity and was capped with a microwave vacuum window at the top of the cryostat. The cavity and the tail of the inner pot were protected from thermal radiation by a copper heat shield cooled to liquid-nitrogen temperature.

The microwave cavity, which is shown in Fig. 3, was designed to maximize the thermal conductivity between the liquid helium in the Dewar and the quartz plate upon which the sample was grown. It was made by electroforming copper on an aluminum mandrel. The outside of the cavity was machined to shape and the six holes were drilled down into the outside walls of the cavity. With the cavity soft-soldered to the tail of the inner pot of the Dewar the liquid helium filled these holes. Liquid-helium fills were always done carefully in order to prevent air from condensing in the inner pot and filling the cooling holes. The outside of the cavity was shaped so that there were thin places in the walls to allow the magnetic modulation field needed for ESR measurements to penetrate to the sample. With the cavity at 4.2°K and a 39 cps modulation field, the magnetic field inside the cavity was measured to be 0.5% of the external field. A calculation of the sample heating during deposition at 4.2°K including the radiant heat through the optical access holes in the heat shield gave the temperature at the surface of a 5-mm-thick sample to be less than 5.2°K.

The cryostat was joined to the rest of the vacuum system through a rotating O-ring seal. The sample was grown with the hole in the broad face of the cavity opposite the crystal plate turned toward the oven. The Dewar was then rotated 90° for ESR and optical studies. In this position the $\Delta M=\pm 1$ ESR transitions were observed. ESR studies could also be conducted with the Dewar in the growing position; in this orientation $\Delta M=0$ transitions could be observed.

The vacuum system was evacuated by means of two 60-liter per sec oil diffusion pumps. The ultimate vacuum as measured by an ionization gauge was roughly 5×10^{-7} Torr with the Dewar uncooled. With liquid helium in the inner pot the pressure was a factor of 2 or 3 lower. When the sample was being deposited

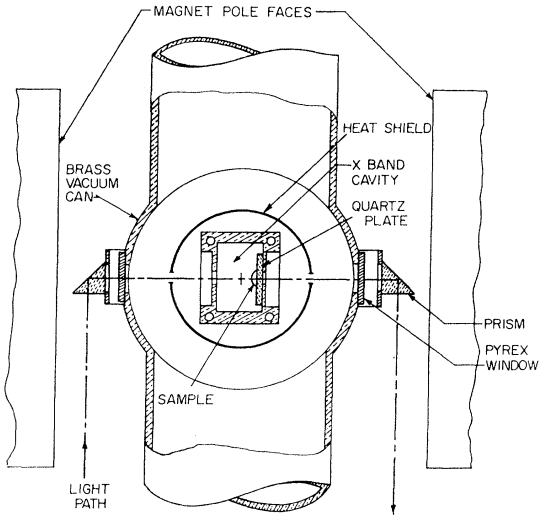

FIG. 5. A sketch showing the method used for obtaining optical access to the sample.

the pressure in the vacuum space rose to 5×10^{-4} Torr. A large mechanical pump was available for pumping on the liquid helium in the inner pot. It was possible to lower the temperature of the liquid helium to 1.3°K for periods of seven or eight hours.

The electromagnet used was designed and constructed under the direction of Professor K. T. Bainbridge. It was fitted with 9-in.-diam, cylindrical pole pieces and Rose shims. The field in the center of the magnet gap varied by less than one part is 10^4 over a cylindrical volume $\frac{3}{4}$ in. in diam by $\frac{3}{8}$-in. deep whose axis was parallel to the axis of the magnet poles. The magnet was equipped with field modulation coils suitable for use in the audio and subaudio range. The field was measured by means of an NMR apparatus.

The ESR spectrometer, which was designed and constructed by Weyhmann,[2] is a phase-locked superheterodyne spectrometer operating at X band. The block diagram is shown in Fig. 4. In this spectrometer the local oscillator is phase-locked 30 Mc/sec away from the signal klystron frequency and a 30 Mc/sec lock-in detector is used to detect the component of the signal frequency which is modulated at the audio magnetic field sweep frequency. This spectrometer has the advantage that one can switch from dispersion to absorption while the bridge is still balanced by using simple microwave phase shifters. For the observations reported in this paper the spectrometer was operated in the dispersion mode.

Since it was desired to make simultaneous optical and ESR measurements on the sample and since observations of the $\Delta M=\pm1$ ESR transitions require that the broad face of the cavity be perpendicular to the dc magnetic field, the method of optical access employed was that shown in Fig. 5. A silvered prism was used to reflect light entering perpendicular to the axis of the magnetic pole faces parallel to the field and through the sample. A similar prism directed the light out from between the pole faces after it had passed through the sample. This method was chosen in preference to drilling holes in the pole faces because of limitations in laboratory space and because of its relative simplicity.

Since it was desired to make measurements with circularly polarized light it was necessary to consider the effect on the light of reflection by a prism. Reflection introduces a shift in the relative phases of the components of the electric vector of the light in and perpendicular to the plane of reflection and an unequal change in the amplitude of these components. Thus, light circularly polarized before reflection will not be circularly polarized after reflection. This problem can be eliminated if light leaving the circular polarizer is reflected through an identical prism whose plane of reflection is oriented so that it is perpendicular to the plane of reflection of the second prism. If this is done the effects mentioned above are cancelled and the light coming out of the second prism will be circularly polarized. In practice it was found that the planes of reflection of the two prisms could be adjusted so that circularly polarized light entering the first prism would emerge from the second prism with the ratio of its minor to its major axis equal to or greater than 0.98. There was a small decrease in this ratio after the light passed through the pyrex vacuum window shown in Fig. 5; measurements at the sample position showed the decrease was less than 5%.

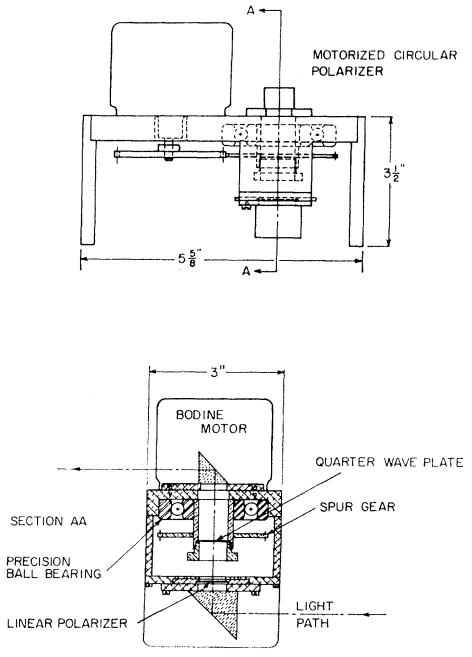

FIG. 6. A drawing showing the construction of the motorized circular polarizer.

The rest of the optical spectrometer consisted of various lenses and prisms, a light source, a monochromator, a circular polarizer, a photomultiplier tube and its power supply, a General Radio electrometer, a lock-in detector, an audio-frequency oscillator, an audio-frequency power amplifier, and a strip chart recorder. The light source used was a General Electric EPR projection-type lamp rated at 6 V, 18 A. It was chosen because of its small filament. For longer life, the lamp was run at 17 A. The current to the lamp was supplied by a regulated dc power supply.

The operation of the optical spectrometer group can be understood from Fig. 2. White light from the light source is focused on the entrance slit of a Jarrell–Ash type 8200 0.5-m Ebert scanning spectrometer furnished with adjustable-width slits and a synchronous motor drive. With the entrance and exit slits set at a width of 65 μ and a 12 000 line/cm grating, the light out of the monochromator had a full width at half-maximum of 13 Å. The light from the exit slit of the monochromator was reflected up to a motorized circular polarizer which consisted of a Polaroid HN 7 linear polarizer followed by a Polaroid retarder plate that was quarter wave at approximately 7800 Å. Since this was a non-standard retardation, the plate was specially selected from batches of 8200 Å quarter-wave plates. The quarter-wave plate was $\frac{5}{8}$ in. in diam and was mounted in the bore of the inner ring of a $\frac{3}{4}$-in.-bore precision ball bearing by means of a brass holder (Fig. 6). The holder was in the form of a tube with an inner step. It was concentric with the inner ring of the ball bearing and was forced into the bore of the inner ring. The quarter-wave plate was held against the step in the holder by means of a screw plug. A spur gear was forced over the outside of the holder and driven by a similar gear attached to a Bodine KYC 26, 1800-rpm, synchronous motor. During motorized circular polarizer (hereafter referred to as MCP) runs, this motor was

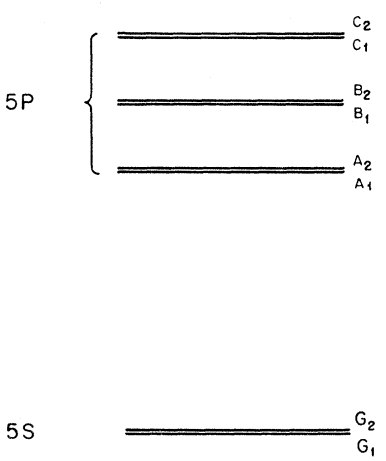

FIG. 7. Energy levels for a rubidium atom in a trapping site. The diagram takes into consideration only the orbital and electron spin angular momentum; the nuclear spin has been neglected.

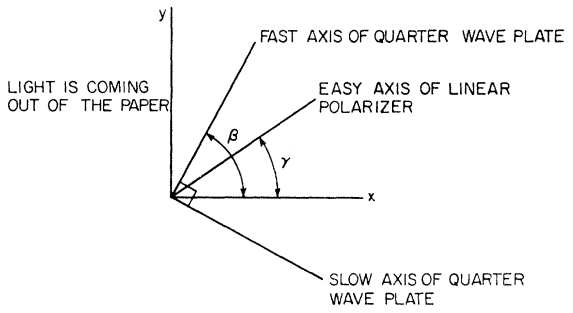

FIG. 8. Diagram showing the angle used to define the orientation of the quarter-wave plate and circular polarizer in the laboratory coordinate system.

run from the same source that supplied the reference frequency for the lock-in detector. In this way, the polarization of the almost monochromatic light passing through the sample was synchronized with the lock-in detector. The method just described was chosen for mounting the quarter-wave plate because it allowed us to use small quarter-wave plates, an important point when it is desired to work in wavelength regions where commercial plates are not easily available. With this set-up it is a trivial matter to change plates and, since the light always passes through the center of the plate, modulation of the light intensity by imperfections in the plate is minimized.

After passing through the MCP the light is conducted to the sample by means of two prisms as was previously described. In a similar manner, the light is conducted by means of two more prisms to an end window photomultiplier tube mounted with its axis vertical. The photomultiplier tube was a Dumont type K1292 with an infrared photocathode. Its response was peaked at 7500 Å and was adequate throughout the wavelength range of interest in this experiment. The tube was magnetically shielded and sufficiently far from the magnet that the effect of the magnetic field on the tube gain was small. Even though the tube was light-shielded, every effort was made to eliminate extraneous light and all runs were made with the room lights out. The output of the phototube was run to the General Radio electrometer and then to an Electronics Missiles and Communications model RJB lock-in detector. The five times full-scale zero suppression of this lock-in detector proved very useful when observing, in the samples, the interaction between microwaves and light.

For optical absorption measurements the dc output of the General Radio electrometer was connected to the recorder. For MCP measurements and measurements of the microwave-light interaction the output of the lock-in detector was recorded. The phototube could be cooled to dry-ice temperature in order to reduce its dark current when making measurements at low light intensity.

With no sample deposited on the quartz plate and the system properly adjusted, the light power into the

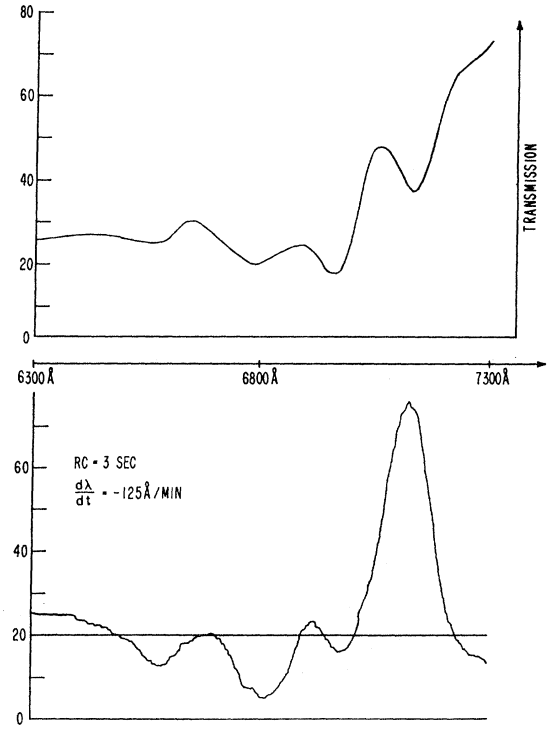

FIG. 9. Recorder tracings showing the optical absorption and the motorized circular polarizer signals as a function of the monochromator wavelength for the shorter-wavelength triplet. The upper trace shows optical transmission; the lower trace shows the motorized circular polarizer signal. For these observations the magnetic field was 7500 G, the temperature 4.2°K and the Rb to Ar ratio 1 to 1000.

phototube with the monochromator set at 8000 Å and its slits set at 65 μ was sufficient to give full scale deflection on the 100-mV scale of the General Radio electrometer when its input impedance was set at 1 MΩ and the phototube voltage was 590 V. This corresponds to a light power into the phototube of 2×10^{-8} W.

DESCRIPTION OF GROUND-STATE RUBIDIUM ATOM

The Hamiltonian for a free rubidium atom in its ground state in the presence of a magnetic field **H** is

$$\mathcal{H}=A\mathbf{I}\cdot\mathbf{J}-g_J\mu_0\mathbf{J}\cdot\mathbf{H}-g_I\mu_0\mathbf{I}\cdot\mathbf{H},$$

where A is the hyperfine interaction constant, g_J is the g factor for the electron, J is the electronic spin, g_I is the nuclear g factor, I is the nuclear spin, and μ_0 is the Bohr magneton. Normal rubidium is 78.15% Rb^{87} and 27.85% Rb^{85}. The nuclear spin of Rb^{85} is $\frac{5}{2}$; the nuclear spin of Rb^{87} is $\frac{3}{2}$. The hyperfine interaction constant for Rb^{85} is 1011.90 Mc/sec; the hyperfine interaction constant for Rb^{87} is 3417.3 Mc/sec. The effect of the argon matrix is to distort the rubidium atom and change its effective hyperfine interaction constant and electronic g factor. It is conventional to characterize this change in terms of the change in the effective hyperfine interaction $\Delta A/A$ from the free-atom value and the change Δg in the effective g factor from the free-atom g factor.

THEORY OF LIGHT ABSORPTION

In this section we will outline the method used to relate the absorption of right and left circularly polarized light to the structure of the trapping sites. The sample will be assumed to consist of a large number of randomly oriented argon microcrystals doped with rubidium atoms. The ratio of the rubidium atoms to argon atoms in the samples was generally in the range of 1 to 1500. This ratio is sufficiently small that the interaction between the different rubidium atoms can be neglected. We will accordingly assume that the light absorption is due to single rubidium atoms and we will use a simple crystal-field model to describe the effect of the argon upon the rubidium.

The absorption spectrum of rubidium in argon consists of triplets in the vicinity of the free-atom $5s$–$5p$ multiplet. The splitting between the components of the triplet is roughly 200 Å. Each of these triplets will be assumed to be due to rubidium atoms in a specific type of trapping site and the triplet structure will be assumed to arise from the effect of the argon atoms on the $5p$ configuration of the rubidium atom. Stationary-state perturbation theory will be used to find the eigenfunctions of the atom and time-dependent perturbation

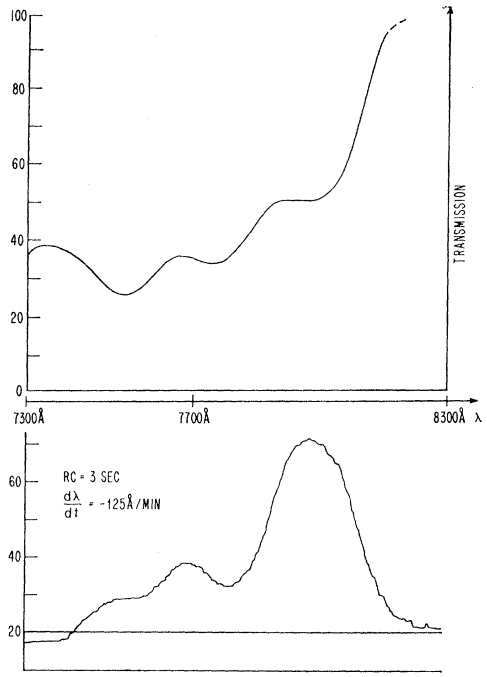

FIG. 10. Recorder tracing showing the optical absorption and the motorized circular polarizer signals as functions of wavelength for the longer-wavelength triplet. The upper trace shows the optical transmission; the lower trace shows the motorized circular polarizer signal. For these observations the magnetic field was 7500 G, the temperature 4.2°K and the Rb-to-Ar ratio 1 to 1000.

theory will be used to find the absorption probability. Throughout this calculation we will assume the nuclear spin is zero.

The assumed Hamiltonian for the stationary-state perturbation calculation is

$$\mathcal{H}=p^2/2m+V(r)+\lambda\mathbf{L}\cdot\mathbf{S}+V(r,\theta,\varphi). \quad (1)$$

Here $p^2/2m$ is the kinetic energy, $V(r)$ is the central potential determined by the nucleus and the closed-shell electrons of the rubidium atom, $\lambda\mathbf{L}\cdot\mathbf{S}$ is the spin-orbit interaction for the free atom, and $V(r,\theta,\varphi)$ is the crystal-field potential. Since for rubidium in argon the spin-orbit splitting is of the order of the triplet splitting in the solid and each of these is smaller than the energy separation of adjacent atomic rubidium configurations, we will treat the last two terms of Eq. (1) as a perturbation. The eigenfunctions are found by diagonalizing the submatrix that corresponds to the $5p$ configuration. The perturbation matrix is formed from the matrix elements of the last two terms of Eq. (1) using the zeroth-order $5p$ eigenfunction in the (L, M_L, S, M_S) representation. The procedure for obtaining the matrix elements is straightforward for the spin-orbit terms. To obtain the matrix elements of $V(r,\theta,\varphi)$ we expand the potential in a series of spherical harmonics. The angular momentum properties of the $5p$ eigenfunctions and of the spherical harmonics, considerations of parity, and the requirement that the crystal-field potential be real dictate that the only terms in the expansion of the potential that give nonzero matrix elements are[9]

$$a_0+a_2^0Y_2^0+a_2^1(Y_2^1+Y_2^{-1})+a_2^2(Y_2^2+Y_2^{-2}). \quad (2)$$

These coefficients are the only ones accessible through investigations involving an $L=1$ orbital angular momentum state.

In the usual perturbation problem, the perturbation matrix is known and the energy values of the perturbed levels are found from the secular equation. In the present case, the energies of the perturbed levels are known from absorption measurements and the coefficients of the crystal-field expansion are to be found. There are, however, four coefficients in the potential (2) and only two independent pieces of information,

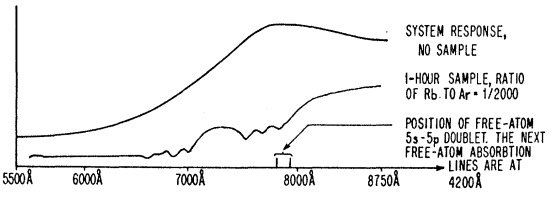

FIG. 11. Sketch showing the system response with no sample, the absorption spectrum for a 1-hour sample and the relative position of the free-atom $5s$-$5p$ doublet.

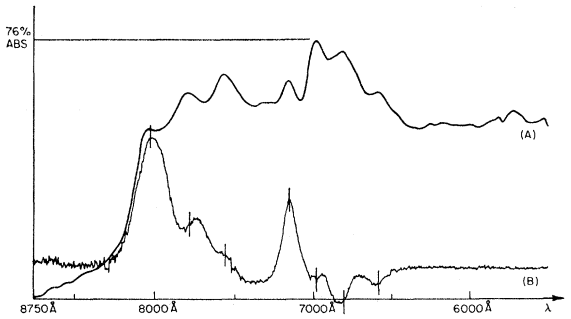

FIG. 12. Drawing showing a comparison between the absorption signal (A) and the motorized circular polarizer signal (B). The absorption signal has been corrected for system response and plotted so that the ordinate is proportional to the relative absorption. The small vertical lines on the motorized circular polarizer recording show the position of the corresponding absorption lines.

namely, the two independent splittings of a triplet. Since a_0 has no connection with the line splitting of a given triplet it may be set aside. However, we are still left with one too many unknowns for a straightforward solution of the problem. The simplest way to proceed is to assume that one of the three remaining coefficients will be equal to zero. We can then solve for the two nonzero coefficients. This procedure will yield several sets of values for each of the two nonzero coefficients. Each set of coefficients can be used to calculate a set of eigenvectors which can be associated with the perturbed energy levels. However, since all but one set of coefficients are spurious, arising in the algebra of the solution of the secular equation, only one set of eigenvectors can have physical meaning. What is needed at this point is some observable characteristic that can discriminate between the different sets of eigenvectors. The difference in the ability of atoms with a nonzero electronic ground-state polarization to absorb right and left circularly polarized light is one such characteristic. Under these conditions the differential absorption of right and left circularly polarized light depends upon the degree of quenching by the crystal field of the angular momentum in the excited state. Since each set of coefficients gives a set of eigenvectors with different degrees of quenching of the angular momentum, measurements of the differential absorption of circularly polarized light by the different lines of a triplet can discriminate between the alternate solutions.

The light absorption calculation is carried out as follows. The rubidium atoms are assumed to be illuminated with plane-wave, circularly polarized light. The interaction between the light and the trapped atoms is described by the interaction Hamiltonian[10]

$$\mathcal{H}_I=(e/mc)\mathbf{p}\cdot\mathbf{A}. \quad (3)$$

Here $\mathbf{A}$ is the vector potential for the light wave. The level scheme for the $5s$ and $5p$ configurations is shown

[9] E. Fick and G. Joos, *Handbuch der Physik*, edited by S. Flügge (Springer–Verlag, Berlin, 1951), Vol. XXVIII, pp. 205–295.

[10] L. I. Schiff, *Quantum Mechanics*, (McGraw-Hill Book Co., Inc., New York, 1955), p. 249.

TABLE I. Observed absorption maxima of the rubidium centers as determined from the optical absorption and motorized circular polarizer measurements. The relative intensities are crude and are only given to suggest the relative size of the signals.

General designation	Line position in Å: As measured in absorption	Line position in Å: As measured by MCP	Relative intensity in absorption mode	Relative intensity in MCP mode
Red triplet	7981±25	7979±25	1	1
	7748±14	7695±14	1	0.35
	7539±15	7542±15	1	0.07
Blue triplet	7130±11	7120±11	1	0.52
	6961±11	6918±11	1	0.07
	6788±13	6806±13	1	0.29
	6566±10	6583±10	1	0.10

in Fig. 7. G, A, B, and C are all Kramers doublets, degenerate in the absence of a magnetic field. A, B, and C are the excited levels belonging to the $5p$ configuration and G is the $5s$ ground level. The three lines observed in connection with each trapping site result from the transitions G–A, G–B, and G–C. The probability that one of these transitions will occur is equal to the sum of the probabilities of all possible transitions between the states of the two levels involved. Time-dependent perturbation theory gives, to first order, the probability of a transition per unit time from a state of the ground level G_l to a state of an excited level E_m to be

$$P(G_l \rightarrow E_m) = \frac{2\pi e^2[\omega(G_l \rightarrow E_m)]^2}{c^2 h^4} \mid \mathbf{A}_c \cdot \langle G_l \mid \mathbf{r} \mid E_m \rangle \mid^2. \tag{4}$$

$\mathbf{A}_c$ is a complex bivector and is a function of the orientation of the fast axis of the quarter-wave plate, the transmission axis of the linear polarizer, the amplitude and the wavelength of the incident plane wave and the wavelength at which the plate is a quarter-wave plate. The $\mid E_m \rangle$ are known from the stationary-state calculation and the $\mid G_l \rangle$ are the unperturbed eigenvectors of the ground state in the (n, L, M_L, S, M_S) representation for which $n=5$, $L=0$, and $S=\frac{1}{2}$. We take account of the random orientation of the sites by transforming the vector potential of the incoming plane wave into the coordinate system of the trapping site by means of the Euler angles. The laboratory coordinate system is chosen so that the magnetic field lies along the z axis and the vector potential lies in the x–y plane. The Euler angles used are those that would be used to rotate the laboratory coordinate system so that it coincides with the coordinate system of the site. The convention of Goldstein[11] is used for the Euler angles. With this convention the first rotation $(x, y, z \rightarrow \xi, \eta, \zeta)$ is through an angle φ about the z axis of the laboratory system; the second rotation $(\xi, \eta, \zeta \rightarrow \xi', \eta', \zeta')$ is through an angle θ about the ξ axis; the third rotation $(\xi', \eta', \zeta' \rightarrow x', y', z')$ is through an angle ψ about the ζ' axis.

The orientation in the laboratory coordinate system of the quarter-wave plate and the linear polarizer is shown in Fig. 8. The light is right circularly polarized when the angle $\beta-\gamma$ between the easy axis of the polarizer and the fast axis of the quarter wave plate is $\pi/4+n\pi$ and left circularly polarized when this angle is $-\pi/4+n\pi$.

The action of the low temperature and the magnetic field on the trapped rubidium atoms produces a difference in the population of the two states of the ground

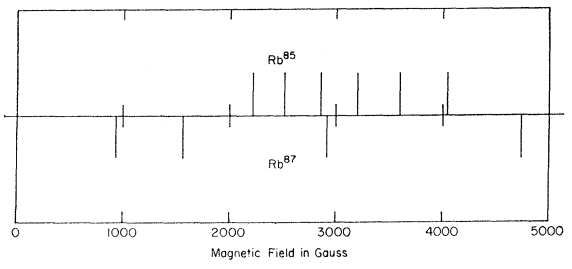

FIG. 13. Diagram showing the relative position of the Rb^{85} and Rb^{87} $\Delta M = \pm 1$ electron spin resonance lines as a function of magnetic field for a klystron frequency of 9000 Mc/sec.

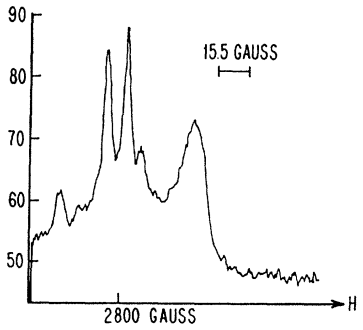

FIG. 14. A chart recording showing the electron spin resonance in the vicinity of 2800 G. When these data were taken the Rb-to-Ar ratio was 1 to 2500, the temperature was 4.2°K, the lock-in detector time constant was 0.3 sec and the rate of field sweep was 41 G/min.

[11] H. Goldstein, *Classical Mechanics* (Addison-Wesley Publishing Co., Inc., Reading, Mass., 1959).

TABLE II. The observed position of the principal ESR lines in the 3600-G region for a klystron frequency of 8953 Mc/sec and the shifts in the hyperfine interaction constant $\Delta A/A$ and g factor (Δg) of the free atom required to fit the data. For this frequency the free-atom lines should appear at 3603.7 and 3600.7 G.

Designation of line	Observed position in gauss for klystron frequency of 8953 Mc/sec.	Full width at half-max.	$100(\Delta A/A)$	$10^3\,\Delta g$
A	3603.1±0.25	7.5	−0.53±0.11	−1.3 ±0.30
B	3622.9±0.25	4.0	6.08±0.36	−2.43±0.14
C	3627.2±0.25	4.0	7.71±0.38	−2.39±0.12

level. For sites whose positive z axis is pointing along the magnetic field, the probability that an atom in the ground state will have its electron spin pointing in the positive z direction is given by

$$\omega_2=\frac{\exp(-\mu_0 H/kT)}{2\cosh(\mu_0 H/kT)}, \tag{5}$$

and the probability that the electron spin will point in the negative z direction is given by

$$\omega_1=\frac{\exp(\mu_0 H/kT)}{2\cosh(\mu_0 H/kT)}. \tag{6}$$

Here H is the magnetic field and μ_0 is the Bohr magneton. For a site whose orientation is given by the Euler angles θ, φ and ψ, the energy eigenvectors for the ground state can be written in the form

$$|G_2\rangle=\cos\tfrac{1}{2}\theta\,|G_2^0\rangle+i\exp(-i\psi)\sin\tfrac{1}{2}\theta\,|G_1^0\rangle, \tag{7}$$

$$|G_1\rangle=i\exp(i\psi)\sin\tfrac{1}{2}\theta\,|G_2^0\rangle+\cos\tfrac{1}{2}\theta\,|G_1^0\rangle. \tag{8}$$

$|G_2^0\rangle$ and $|G_1^0\rangle$ are the states for which the spin points along and opposite to the positive z axis of the site, respectively, while $|G_2\rangle$ and $|G_1\rangle$ describe states with spins pointing along and opposite to the magnetic field. Thus the probability of finding an atom in the ground level in the state $|G_2\rangle$ is ω_2 and the probability of finding it in $|G_1\rangle$ is ω_1. The probability per unit time that the atom in a randomly oriented trapping site will absorb a photon is given by $\omega_i P(G_i\rightarrow E_m)$ where $i=1$ or 2 depending on the orientation of the ground-state electron relative to the magnetic field. From Fig. 7

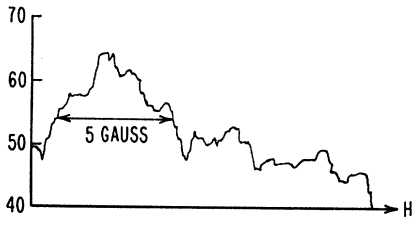

FIG. 15. A chart recording showing the interaction line in the 3600 G region. This observation was made by sitting on the MCP line at 7130 Å and then saturating the microwave transition in the vicinity of 3600 G. The Rb-to-Ar ratio was 1 to 1000, the temperature 4.2°K, the lock-in detector time constant 10 sec and the rate of field sweep 4.1 G/min.

we see that there are three excited levels, A, B, and C, available and in each level the states 1 and 2. The probability of an absorption per unit time from the ground level to one such level E is

$$T(G,E)=\frac{2\pi e^2[\omega(G,E)]^2}{c^2h^4}\sum_{l=1,2;m=1,2}|\mathbf{A}_c\cdot\langle G_l|\,\mathbf{r}\,|E_m\rangle|^2\omega_l. \tag{9}$$

Here we have assumed $\omega(G_l\rightarrow E_m)=\omega(G,E)$, since for the maximum magnetic fields used in this experiment the splitting due to the magnetic field is less than $\frac{1}{2}$ Å.

Since the sample consists of a large number of rubidium atoms in randomly oriented trapping sites, the average absorption probability for all of the atoms in a particular type of site will be found by averaging $T(G,E)$ over the Eulerian angles. Let us call this probability $T(G,E,\beta-\gamma)$. The ratio of the absorption by the atoms of right and left circularly polarized light is then given by

$$\delta(G,E)=\frac{T(G,E,\pi/4)}{T(G,E,-\pi/4)}. \tag{10}$$

We will obtain a set of values of $\delta(G,E)$ for each set of crystal-field coefficients. Comparison of the measured values of $\delta(G,E)$ with the calculated values can tell us which set of crystal-field coefficients is the proper set.

If the eigenfunctions of the trapped rubidium atom in the excited p state are written in the form

$$|E_k\rangle=\sum_{m_l=-1,0,1;m_s=-1/2,1/2}|1,m_l,\tfrac{1}{2},m_s\rangle\langle 1,m_l,\tfrac{1}{2},m_s\,|\,E_k\rangle,$$

where $E=A$, B or C and $k=1$ or 2, then it can be shown that the general expression for $T(G,E,\pi/2)$ is

$$\begin{aligned}T(G,E_k,\pi/2)=C[1+\tfrac{1}{2}(\omega_+-\omega_-)\sin(\beta-\gamma)\sin(\tfrac{1}{2}\pi\lambda_0/\lambda)\\ \times\{|\langle 1,-1,\tfrac{1}{2},\tfrac{1}{2}\,|\,E_1\rangle|^2+|\langle 1,1,\tfrac{1}{2},-\tfrac{1}{2}\,|\,E_1\rangle|^2\\ -|\langle 1,1,\tfrac{1}{2},\tfrac{1}{2}\,|\,E_1\rangle|^2-|\langle 1,-1,\tfrac{1}{2},-\tfrac{1}{2}\,|\,E_1\rangle|^2\\ -\sqrt{2}\langle 1,0,\tfrac{1}{2},-\tfrac{1}{2}\,|\,E_1\rangle\\ \times(\langle 1,-1,\tfrac{1}{2},\tfrac{1}{2}\,|\,E_1\rangle-\langle 1,1,\tfrac{1}{2},\tfrac{1}{2}\,|\,E_1\rangle)\\ -\sqrt{2}\langle 1,0,\tfrac{1}{2},\tfrac{1}{2}\,|\,E_1\rangle\\ \times(\langle 1,1,\tfrac{1}{2},-\tfrac{1}{2}\,|\,E_1\rangle-\langle 1,-1,\tfrac{1}{2},-\tfrac{1}{2}\,|\,E_1\rangle)\}].\end{aligned} \tag{11}$$

TABLE III. The calculated values for the differential absorption of right and left circularly polarized light for the various sets of crystal-field parameters that fit the observed splittings. In each case it has been assumed that the site has a twofold axis of symmetry, so that the only relevant terms in the crystal-field expansion are a_2^0 and a_2^2.

General designation	Transition	Crystal-field parameters a_2^0	a_2^2	$100[\delta(G,E)-1]$ differential absorption of right and left circularly polarized light Theoretical	Experimental
Red triplet	G–A	1190	385	10.5	3.70±0.7
	G–B			−9.5	1.30±0.22
	G–C			−1.8	0.74±0.15
	G–A	−120	925	10.5	3.70±0.7
	G–B			−8.7	1.30±0.22
				−1.9	0.74±0.15
	G–A	−1070	540	8.2	3.70±0.7
	G–B			−4.1	1.30±0.22
	G–C			−4.0	0.74±0.15
Blue triplet	G–A	2120	1048	4.8	2.98±0.6
	G–B			−3.5	−2.41±0.46
	G–C			−1.1	−2.37±0.74
	G–A	220	1830	4.8	2.98±0.6
	G–B			−7.4	−2.41±0.46
	G–C			−1.2	−2.37±0.74
	G–A	−2350	765	2.8	2.98±0.6
	G–B			0.14	−2.41±0.46
	G–C			−3.3	−2.37±0.74

Here C is a constant and E is one of the three Kramer doublets A, B, or C.

PROCEDURES FOR TAKING DATA

Two types of samples, which differed only in the amount of material deposited on the cooled quartz plate, were grown. Optical samples were deposited for times ranging from half an hour to several hours; they had 30 to 60% light absorption due to the argon and 50 to 95% light absorption at the centers of the rubidium lines. The ESR samples were grown until an adequate signal was obtained; the times ranged from 6 to 36 h. ESR samples were often grown on top of optical samples. For both optical and ESR samples the concentration of rubidium in the rubidium argon gas mixture was usually set in the range from 1 in 1000 to 1 in 2000. Occasional runs were made with higher and lower concentrations. The rubidium used was 99.9% pure; the argon was high-purity commercial grade, 99.998% pure. The argon was passed through a charcoal trap cooled to dry-ice temperature to further eliminate impurities.

It is difficult to know the concentration of active rubidium atoms in the sample itself because of lack of knowledge of the sticking coefficient of rubidium on argon and the processes taking place on the surface of the growing sample. Another cause of uncertainty is the wall of the vacuum chamber, which was at room temperature, between the oven and the Dewar; rubidium atoms that struck the wall would tend to stick while argon atoms would bounce off. All of these processes tend to lower the concentration of active rubidium atoms in the sample. Measurements by Weyhmann of the broadening of the ESR lines of sodium trapped in argon indicate a reduction in concentration of active metal atoms of from two or three to an order of magnitude.

Prior to growing a sample, scans were made with the optical spectrometer in both the absorption and motorized circular polarizer (MCP) modes and with the ESR spectrometer in order to determine the system response without a sample. At intervals the growing was temporarily stopped and the sample was checked to see if it was adequate. Typical strip chart recordings showing the data for the optical absorption spectrometer, and the MCP spectrometer are shown in Figs. 9 and 10. The optical spectrometer recordings give the intensity of the light passing through the sample as a function of wavelength. The MCP recordings give the differential absorption of right and left circularly polarized light as a function of wavelength. The nuclear resonance detector was used to measure the magnetic field at each of the ESR lines. Figure 11 shows for the optical absorption the system response with no sample, the absorption spectrum with one hours growth, and the relative position of the $5s$–$5p$ doublet of the free rubidium atom.

The experimental values of $\delta(G,E)$ defined in Eq. (10) were determined from the MCP and absorption data using the expression

$$\delta(G,E)_{\text{exp}}=1-\ln\frac{1+\frac{1}{2}(Q_D/Q_A)}{1-\frac{1}{2}(Q_D/Q_A)}\Big/\ln\frac{R_{\text{Ar}}}{R}. \quad (12)$$

Here Q_A is the output of the phototube as read on the electrometer when the spectrometer is set at the center of the G–E line and Q_D is the difference in the number of right and left circularly polarized photons of wavelength $\lambda_{G,E}$ passing through the sample as measured

on the lock-in amplifier and converted to electrometer scale units. Thus

$$Q_D/Q_A=(I_R-I_L)/[\tfrac{1}{2}(I_R+I_L)], \qquad (13)$$

where I_R and I_L are the intensity of the right and left circularly polarized light passing through the sample. In Eq. (12), R is the ratio of the average number of photons of wavelength λ_{GE} arriving at the phototube after passing through the sample to the number arriving at the phototube before the sample was grown. R_{Ar} is this ratio for the loss in intensity due to the argon only. R_{Ar} was determined by measuring the intensities far from the position of any rubidium lines before and after the sample was grown. Measurements showed that this ratio varied slowly with wavelength and was a constant over any one triplet. Equation 12 assumes that the number of right and left circularly polarized photons produced by the MCP were equal and that the I_R-I_L was never more than a few percent of the average intensity. Measurements showed that both these assumptions are justified.

RESULTS

Figure 12 shows on the same scale a comparison between the optical absorption signals and the motorized circular polarizer signals. Graphs such as these were used to determine the position of the lines. Table I shows the position of the optical absorption lines determined from both the absorption and the MCP measurements. The positions of the optical absorption lines determined from measurements at 4.2 and 1.3°K agreed to better than 7 Å in all cases. The positions of the lines as determined from the absorption and MCP measurements did not agree in all cases; in one case they differed by as much as 50 Å. This disagreement is thought to be due to the fact that the lines are not well resolved. Four lines were found in the blue group. It is not clear whether there are two triplets, a triplet and a doublet, or two doublets. In comparing experimental and theoretical values of $\delta(G, E)$ it has been assumed that the three most prominent blue lines form a triplet. The full width at half-maximum of the absorption lines is estimated to be 150 Å (250 cm^{-1}).

The expected positions of the rubidium $\Delta m=\pm 1$ ESR lines calculated using the Breit–Rabi formula are shown in Fig. 13. Figure 14 shows the paramagnetic resonance lines in the vicinity of 2800 G. ESR lines were observed in the 2200-, 2500-, 2800-, 3600-, and 4050-G regions. No lines were seen in the 4700-G region where one expects only Rb^{87} lines. In all cases the line families were similar; there was no evidence for the Rb^{87} lines even in the 2800-G region where the free-atom lines of the two isotopes are close together.

In each region there were three major lines and two smaller lines. The three major lines consisted of a broad singlet and a doublet formed of two narrower lines. The broad line was found to be close to the position of the free-atom line. The structure of the three major lines is very similar to that found by Weyhmann for sodium in argon. The departures of g_i and ν_{hfs} from the free-atom values for Rb^{85} were calculated using the Breit–Rabi formula and the shift of the lines from the calculated free-atom positions. These shifts are given in Table II along with the calculated and observed positions for the three major lines and the observed linewidths in the 3600-G region.

In order to correlate the optical absorption and ESR sites, each MCP line was monitored and the ESR transitions were successively saturated. It was expected that the amplitude of the MCP line would be reduced when an EPR line associated with the same site partially equalized the population of the ground-state energy levels. Such lines will be called interaction lines. An effect was found only for the 7130 Å line. Figure 15 shows this particular interaction line. No effect was seen in the larger 7981 Å line or the other small MCP lines. Since a sample thick enough for ESR observations was too thick for MCP observations, the ESR and interaction lines were correlated by first finding the interaction line and then growing the sample thick enough so that the ESR line could be seen. In this manner the 7130 Å line was found to be associated with the major ESR line farthest from the broad line. This is called line C in Table II.

Since the amplitude of the interaction line did not change with the microwave power level at the highest power level used, it was concluded that the ESR lines could be saturated. Since the amplitude of the interaction line did not change with the amplitude of the modulation field, it was concluded that the ESR line associated with the 7130 Å optical line was homogeneously broadened. The size of the interaction line when the ESR lines were saturated was roughly 5% of the MCP line. The signal-to-noise ratio was roughly 5 to 1.

Table III shows a comparison of the experimental and theoretical values of $\delta(G, E)$ for the red triplet and the triple formed from the three most prominent blue-shifted MCP lines. For these theoretical calculations it was assumed that the trapping site had a twofold axis of symmetry and thus that the coefficient a_2^1 of Eq. (2) was zero. Table III shows that two out of three of the possible sets of coefficients give reasonable agreement with the blue shifted triplet. For the red triplet the agreement is poor for all of the possible sets of coefficients.

There is a considerable uncertainty in these theoretical predictions due to the uncertainty in the splittings which shows up as an apparent difference between the positions of the absorption and MCP lines and due to the strong dependence of the values of $\delta(G, E)$ on these splittings. The theoretical results should be regarded more as a qualitative factor of 2 result than an exact quantative prediction. A great deal more work is required to make a detailed prediction.

DISCUSSION

In this section we shall consider the information derived from this experiment and other experiments on alkali centers in rare-gas crystals and try to obtain a coherent picture of the trapping sites.

Some of the relevant observations concerning the sites are the following:

(1) The stability of the sites when the samples are warmed up and the reproducibility of the sites from experiment to experiment suggest that the sites are stable configurations in which the alkali atom is surrounded by rare-gas atoms rather than located on an interface or dislocation.

(2) The narrowness of the paramagnetic resonance lines and the fact that in some cases the transitions have been reported to be homogeneously broadened gives additional evidence for the well-defined structure of the sites.

(3) The fact that the red triplet is close to the free-atom lines and that the blue triplet is not shifted far from the free-atom lines suggests that the sites are loosely bound compared to a substitutional site. This evidence is confirmed by calculations based on a configuration coordinate model and the known Lennard-Jones potential for alkali-atom–rare-gas-atom interactions.

(4) Except for the exceptional site found by Goldsborough and Koehler when they irradiated the growing sample with infrared radiation the g factor shifts and the shifts in the hyperfine interaction constant are not large.

(5) The fact that in all cases the dominant structure consists of triplets and that the relative intensity of the different members of a given triplet does not change even when the growth conditions are such as to eliminate another triplet attests to the stability of the sites and shows that the symmetry of the sites is sufficiently low that the orbital degeneracy of the excited state is completely removed.

(6) The interaction line observed in this experiment shows that the blue triplet has, as one would expect, a large positive hyperfine shift and a large g factor shift. This shows that the ESR and optical sites are related in a logical fashion.

(7) The observation of the absorption of circularly polarized light made in this experiment shows that the orbital angular momentum in the excited state is only partially quenched.

All of these facts can be explained with substitutional sites in which one or more of the nearest-neighbor rare-gas atoms are missing. The lattice then readjusts so as to give as much room as possible to the alkali atom. The excited states have a characteristic lattice distortion for each of the three p orbitals. In order to progress further with the model it is necessary to make detailed calculations in which one considers the coupled atom-lattice system.[12]

ACKNOWLEDGMENTS

We would like especially to acknowledge the aid of Dr. Walter Weyhmann. Dr. Weyhmann built the paramagnetic resonance spectrometer and most of the equipment used to grow the samples. Without the aid of the Jefferson machine shop and the Jefferson carpenter shop this work would have been impossible; we deeply appreciate their aid.

---

[12] For related problems in the analysis of F centers see as examples: P. R. Moran, Phys. Rev. **137,** A1061 (1965); N. V. Karlov, J. Margerie, and Y. Merle D'Aubigne, J. Phys. (Paris) **24,** 717 (1963); J. Mort, F. Luty, and F. C. Brown, Phys. Rev. **137,** A566 (1965); C. H. Henry, S. E. Schnatterly, and C. P. Slichter, *ibid.* **137,** A583 (1965).